Electronic Journal of Biotechnology 56 (2022) 22–30

Contents lists available at ScienceDirect

Electronic Journal of Biotechnology

journal homepage:

Research Article

# One-pot synthesis of UV-protective carbon nanodots from sea cauliflower (*Leathesia difformis*)

Kyung Woo Kim [a,*], Yong Min Kwon [b], Sun Young Kim [a], Jaoon Young Hwan Kim [a]

[a] Department of Applied Research, National Marine Biodiversity Institute of Korea, 75 Jangsan-ro, 101 Beon-gil, Janghang-eup, Seocheon-gun, Chungcheongnam-do 33662, South Korea
[b] Department of Genetic Resources Research, National Marine Biodiversity Institute of Korea, 75 Jangsan-ro, 101 Beon-gil, Janghang-eup, Seocheon-gun, Chungcheongnam-do 33662, South Korea

## GRAPHICAL ABSTRACT

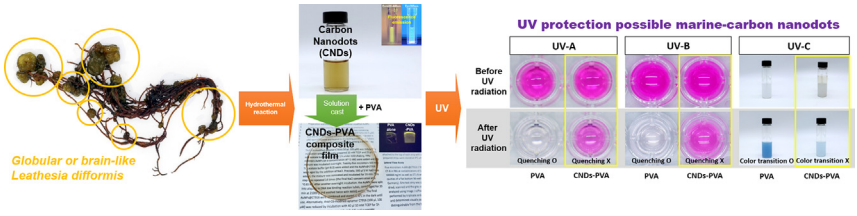


## ARTICLE INFO

*Article history:*
Received 18 July 2021
Accepted 29 December 2021
Available online 4 January 2022

*Keywords:*
Brown algae
Carbon nanodots
Hydrothermal synthesis
*Leathesia difformis*
Marine carbon nanodots
One-pot synthesis
Sea cauliflower
UV radiation
UV rays
UV-blocking carbon nanodots
UV-protective carbon nanodots

## ABSTRACT

*Background:* The interest in ultraviolet (UV) radiation from the sun and artificial sources has been recently increasing due to its toxic effects, including sunburn, erythema, photodamage, and photocarcinogenesis. In this study, we aimed to develop a valuable nanomaterial that can block total UV rays using an undervalued, yet profitable marine organism. We successfully developed carbon nanodots (CNDs) and a CNDs-polyvinyl alcohol (PVA) composite film that effectively protect against UV-A, UV-B, and UV-C radiation based on a common brown algae, sea cauliflower (*Leathesia difformis*), through simple hydrothermal synthesis in aqueous solution.
*Results:* CNDs-PVA film protected rhodamine B from photobleaching and polydiacetylene vesicles with 10,12-tricosadiynoic acid from polymerization. As-fabricated CNDs in aqueous solution blocked >99% of UV-A light, which causes photoaging and skin cancer. The CNDs-PVA film showed excellent transparency, with >84% transmittance of visible light, and effectively blocked >60% of UV-A/B and >30% of UV-C rays under direct and strong irradiation.
*Conclusions:* This preliminary work indicates that CNDs based on underutilized marine brown algae have strong potential for application in technologies for wide UV protection.
**How to cite**: Kim KW, Kwon YM, Kim SY, et al. One-pot synthesis of UV-protective carbon nanodots from sea cauliflower (*Leathesia difformis*). Electron J Biotechnol 2022;56. https://doi.org/10.1016/j.ejbt.2021.12.004


## 1. Introduction

Ultraviolet (UV) radiation from the sun can have various hazardous health effects, including skin phototoxicity, premature aging, eye damage, and carcinogenesis [1]. UV radiation is subdivided into UV-A (320–400 nm), UV-B (280–320 nm), and UV-C

Peer review under responsibility of Pontificia Universidad Católica de Valparaíso
* Corresponding author.
*E-mail address:* kimkw79@mabik.re.kr (K.W. Kim).

https://doi.org/10.1016/j.ejbt.2021.12.004
0717-3458/

(100–280 nm). UV-C is effectively absorbed by atmospheric ozone; thus, humans are predominantly affected by solar UV-A and UV-B [2]. As UV-A light is barely absorbed in the ozone layer, it accounts for 95% of solar UV radiation and is present all day [1]. UV-A is recognized as a major factor causing photoaging and skin cancer as it penetrates the deeper human skin layers, including the epidermis and dermis. Long-term exposure to UV-A noticeably enhances immunosuppression, leading to inflammation and the overproduction of reactive oxygen species (ROS), resulting in photoaging and the development of skin cancer [2,3,4]. Furthermore, UV-A induces the depletion of non-enzymatic and enzymatic antioxidants and initiates DNA damage. UV-A activates the neuroendocrine system responsible for immunosuppression. The accumulation of oxidative lipids, proteins, and carbohydrates resulting from inflammatory responses as well as high ROS levels in the dermis and epidermis can finally lead to photoaging and skin cancer [5,6,7]. According to the official website of the World Health Organization (WHO), the incidence of non-melanoma and melanoma skin cancers has increased over the last few decades, and solar UV radiation causes more than 60,000 deaths each year. WHO experts assume that the recent increase in the incidence of skin cancers is associated with an increase in outdoor recreational activities.

However, skin cancer can largely be prevented by protecting the skin against overexposure to solar UV radiation. Accordingly, various nanoparticles for photoprotection have been developed. Owing to their very small size and large surface area-to-volume ratio, nanoparticles more effectively block UV light than natural materials [8]. Inorganic and organic nanoparticles are two major types of photoprotective agents approved by the US Food and Drug Administration for industrial application [9]. The most widely used inorganic UV reflective sunscreen materials are micron-sized particles of zinc oxide (ZnO) and titanium dioxide ($TiO_2$) [2]. They penetrate less deeply into the dermis than organic particles but have been shown to enhance ROS generation after UV exposure and are capable of inducing cell damage and carcinogenesis [10,11,12]. In addition, ZnO- and $TiO_2$-based commercial sunblock products are non-transparent because of the large particle size [3]. Organic UV-absorbing sunscreen materials include benzophenones, dibenzoylmethanes, salicylates, camphor derivatives, *p*-aminobenzoic acid, and cinnamates. Both inorganic and organic sunscreen ingredients have progressively accumulated as pollutants in marine ecosystems due to the washing off of enormous amounts of sunscreen from human skin every year. For example, sunscreen chemicals have been linked to coral bleaching and oxidative stress in phytoplankton [13,14,15]. In Hawaii, some organic sunscreen agents, such as benzophenone-3 and octyl methoxycinnamate, are banned as of 2021 to preserve marine ecosystems [16]. Over the past few years, many research groups have attempted to develop UV-blocking nanomaterials that are less toxic and more environmentally friendly.

Carbon nanodots (CNDs) are such functional nanomaterials that have many favorable and unique optical properties [17,18,19,20]. CNDs can be generated using uncomplicated methods and they produce fluorescence after excitation with light over a broad range of wavelengths, including the UV region, have good photostability and negligible toxicity towards eukaryotic cells, and are quite environmentally friendly [21,22,23]. As with metallic nanoparticles, including ZnO and $TiO_2$, CNDs can be synthesized by both top-down and bottom-up processes. Top-down processes start from macroscopic graphite, soot, and activated charcoal, and CNDs can be generated by arc discharge, laser ablation, electrochemical oxidation, chemical oxidation, or other methods [23,24,25]. Bottom-up processes use various organic precursors, including natural resources such as watermelon peels, coriander leaves, egg yolk, and even hair fibers, and CND fabrication methods include thermal decomposition, microwave irradiation, and hydrothermal treatment [23,24,25,26]. Interestingly, the synthesis of multipurpose CNDs based on marine resources, such as chitosan, a polysaccharide from marine fish, and extract from brown macroalgae, is often reported [26,27,28].

Recent studies have revealed that CNDs and CNDs-containing composite materials are attractive potential materials for UV protection [17,19,20,29,30]. They have shown that CNDs have the potential to produce multifunctional sun-protective agents. However, in most cases, CNDs were synthesized using a commercial chemical, such as citric acid, or frequently used natural source, such as *Dunaliella salina*, as a starting material. In this study, we aimed to examine whether an insignificant marine resource may have potential for scientific or industrial applications.

Here, we report the one-pot synthesis of UV-blocking CNDs from sea cauliflower (*Leathesia difformis*) using a hydrothermal method and development of a UV-protective transparent CNDs-poly (vinyl alcohol) (PVA) film. *L. difformis* is a littoral brown algae species (class *Phaeophyceae*, order *Ectocarpales*) that is commonly found in high to low intertidals or in tidepools on semi-exposed shorelines in South Korea. Sea cauliflower attaches to rocks or other seaweeds for growth; however, it is not consumed as food and is used only for research purposes (e.g., extracts for antioxidants) in South Korea. Although various marine species live in the intertidal regions, most of them are under- or unutilized. Additionally, UV-protective transparent films are a major requirement in the packaging industry, as exposure to natural or artificial light can lead to unwanted chemical changes in the constituents of foods, beverages, and drugs, which may affect their intrinsic nature [31]. Therefore, many scientific research developments have been achieved in the packaging industry. For these reasons, we had interested in researching UV protective CNDs based on unutilized marine organisms and its application by a transparent UV protection film and showed the possibility in this research.

## 2. Materials and methods

### 2.1. Materials

*L. difformis* was collected from rock surfaces and tidepools at Nam-myeon, Taean-gun, Chungcheongnam-do (36°35′18.8″ N 126°17′24.0″ E; GPS coordinates: 36.588551, 126.290010). 10,12-Tricosadiynoic acid (TRCDA) monomers were purchased from Alfa Aesar (Ward Hill, MA, USA). UltraPure™ DNase/RNase-Free Distilled Water and Minisart® NML syringe filters were obtained from Invitrogen (Carlsbad, CA, USA) and Sartorius AG (Göttingen, Germany). A Slide-A-Lyzer™ Dialysis Cassette (2 K MWCO) was purchased from Thermo Fisher Scientific (Waltham, MA, USA). Chloroform, PVA with a molecular weight of 89,000–98,000, sodium hydroxide, rhodamine B, and hydrogen peroxide were obtained from Sigma-Aldrich (St. Louis, MO, USA).

### 2.2. Synthesis of CNDs

Twenty grams of *L. difformis* flesh was washed thoroughly under running tap water. The washed flesh was quickly frozen in liquid nitrogen and ground in a mortar. After the addition of 20 mL of ultrapure distilled water, the sample was sonicated for 45 min using a Branson Sonifier® ultrasonic cell disruptor/homogenizer (SFX 550; Emerson, St. Louis, MO, USA) at 25% power. The mixture was transferred into a 25-mL polypropylene-lined hydrothermal synthesis autoclave reactor (TEFIC Biotech Co., Xi′an, China) and heated at 180 °C for 4 h. The reactor was then cooled down to 25 °C, yielding a brown-yellowish solution in the furnace. The solution was serially filtered through 0.8-μm, 0.45-μm, and 0.22-μm Minisart® NML syringe filters and then dialyzed through a dialysis

cassette with a molecular weight cut-off of 2 K at 27 °C for 6 h. To remove unreacted or organic residues, liquid–liquid extraction was performed with chloroform at a volume ratio of 1:1. The solution was ultracentrifuged using an Optima XE-100 ultracentrifuge with a Type 45Ti fixed-angle rotor (Beckman Coulter, Brea, CA, USA) at 88,000× *g* for 40 min. The supernatant, containing CNDs, was collected and stored in the dark at 4 °C until use. The CND solution stored in the refrigerator remained well-dispersed for 546 d, without precipitation or loss of optical characteristics. The concentration of the CND solution was approximately 21.4 mg/mL.

### 2.3. Characterization of the CNDs

Fluorescence spectra and UV–vis absorption spectra were obtained using a FluoroMax-4 spectrometer (HORIBA, Ltd., Kyoto, Japan) and BioSpectrometer® basic (Eppendorf, Hamburg, Germany), respectively. Photoluminescence (PL) emission spectra were measured from 270 nm to 700 nm in 10-nm steps in the excitation range of 250 nm to 550 nm. UV–Vis absorption spectra were measured from 280 nm to 800 nm. To determine the photostability of the CNDs, 3 mL of the CND solution was added to Petri dishes, which were exposed to 365 nm of UV light at 20 mW/cm$^2$ in a dark room for 360 min in the first experiment and 37 h in the experiment 1.4 years later. In that time period, the PL intensity of the CNDs at the excitation wavelength of 370 nm, which is the maximum emission intensity, was measured using a FluoroMax-4 spectrometer (HORIBA, Ltd., Kyoto, Japan) The absolute photoluminescence quantum yield (PLQY) of the CNDs was measured by a FluoroMax-4 spectrometer (HORIBA, Ltd., Kyoto, Japan) with a 3.2-inch internal integrating sphere system, including Horiba Jobin Yvon software, v.3.9.0.1 (HORIBA, Ltd.). Ultrapure distilled water was used as a blank reference because it was also the solvent in which the CNDs were dissolved. The excitation and fluorescence emission spectra of the blank reference and CNDs were obtained at 370 nm with 0.5 s of integration time. Fluorescence photo-images of the CNDs were acquired using an EOS M6 digital camera (Canon, Tokyo, Japan) under excitation with an LED light at 430–440 nm or a UV light at 365 nm. The transmittance of the CNDs-PVA film was measured using an HM-150 haze meter (Murakami Color Research Laboratory, Tokyo, Japan) according to ASTM D1003 (Standard Test Method for Haze and Luminous Transmittance of Transparent Plastics), with an entrance port aperture of 14 mm and exit port aperture of 20 mm. The transmittance of the CND solution for determining the UV blocking ratio was measured in 10-nm steps between 360 nm and 740 nm using a CM-5 spectrophotometer (Konica Minolta, Tokyo, Japan) with a built-in Xenon lamp (D65). High-resolution electron microscopic images were acquired using a JEM-3010 microscope operating at 300 kV (JEOL, Ltd., Tokyo, Japan). The particle sizes of the CNDs were analyzed using the Gatan Microscopy Suite® software, v3.30 (Gatan, Inc., Pleasanton, CA, USA). Fourier-transform infrared (FT-IR) spectroscopy and X-ray photoelectron spectroscopy (XPS) were carried out using a Frontier MIR/FIR system within the range of 400 to 4000 cm$^{-1}$ (PerkinElmer, Inc., Waltham, MA, USA) and PHI5000 VersaProbe III (Ulvac-Phi, Inc., Kanagawa, Japan) with an Al Kα (1486.6 eV) radiation beam (100 μm, 25 W, 15 kV), respectively.

### 2.4. Fabrication of CNDs-PVA film

Ten grams of PVA powder was completely dissolved in 100 mL of ultrapure distilled water at 95 °C under constant stirring. Twenty milliliters of the PVA solution was mixed with 6 mL of CND solution or 6 mL of ultrapure distilled water as a negative control. Both solutions were poured into PTFE Petri dishes (diameter, 100 mm, Cowie technology group Ltd., Middlesbrough, UK) and oven-dried at 50 °C for 7 d. When completely dried, the films were peeled from the Petri dishes and stored in a desiccator at 25 °C until use. However, the film after the experiment for UV-A and C was stored at 25 °C for 1.4 years until the experiment against UV-B without a desiccator.

### 2.5. UV blocking tests of CNDs-PVA film

Diacetylene lipids, such as TRCDA, undergo polymerization into nanovesicles via a 1,4-addition reaction upon exposure to UV-C light of 254 nm [32]. Therefore, TRCDA vesicles were selected as an indicator of UV-C blocking. A 1 mM TRCDA solution was prepared using ultrapure distilled water. Firstly, 3.47 mg of TRCDA monomers was dissolved in 1 mL of chloroform and then the solvent was evaporated to obtain a thin film of monomers under a stream of nitrogen gas. The monomer film was thoroughly mixed with 10 mL of ultrapure distilled water at 80 °C for 15 min. The well-mixed solution was sonicated using an SFX 550 ultrasonic cell disruptor/homogenizer at 25% power for 15 min. Finally, the solution was filtered through a 0.8-μm Minisart® NML syringe filter. The TRCDA vesicle solution was stored at 4 °C overnight. The TRCDA solution was irradiated for 5 min by UV-C light with PVA film or CNDs-PVA film and the result was confirmed. To evaluate the UV-A- and UV-B-protective features of CNDs-PVA film, we used 1% (v/v) rhodamine B solution containing 30% (w/w) hydrogen peroxide. We added 200 μL of rhodamine B solution to each well of 96-well plates and covered the plates with CNDs-PVA film or PVA film. The plates were then placed in dark containers with UV lamps installed at the top and exposed to 365 nm (UV-A) or 302 nm (UV-B) for 3 h. After UV irradiation, the vials of TRCDA and plates of rhodamine B were observed with the naked eye and their color images were obtained using a digital camera to determine the colorimetric response (CR%) values. All experiments were performed three times.

### 2.6. Data analysis

All graphs in this article were prepared using SigmaPlot, v13.0 (Systat Software, Inc., San Jose, CA, USA) and Origin, v8.6 (OriginLab Corp., Northampton, MA, USA). UV blocking ratios were calculated using the formula T = 1 – R, where T is transmittance and R is reflectance. Transmittance was measured from 360 nm to 400 nm in 10-nm steps and converted to reflectance. The reflectance values were considered UV blocking values and were plotted. The measurements were performed in triplicate, with negligible standard deviations. The particle sizes of CNDs were estimated from TEM images using Gatan Microscopy Suite®. Histograms showing the particle size distribution were fitted to a Gaussian function in the program Origin. The CR% was calculated using the formula mentioned further in the text. To this end, color images of PVA film and CNDs-PVA film were acquired using a digital camera and converted to grayscale images using ImageJ v1.51j8 for quantification of the gray levels for the density of blue or red colors obtained by UV blocking tests. Then, bar graphs were plotted for comparison of the samples.

## 3. Results and discussion

### 3.1. Optical and morphological study of the CNDs

A CND aqueous solution was obtained through the hydrothermal reaction of the flesh of natural *L. differmis* followed by multiple purification procedures. The final solution was clear yellowish-brown to the naked eye in daylight. Upon irradiation with LED light of 430–440 nm and UV light of 365 nm, the CND solution turned

light-green and coral blue, respectively (Fig. S1). The UV–vis absorption spectrum had two sharp peaks at 290 nm and 294 nm assigned to $\pi$-$\pi^*$ transition of the C=C bonds in the aromatic $sp^2$ domain and a very weak shoulder peak around 324 nm allocated to n-$\pi^*$ transition of the CND C=O bonds (Fig. 1a). The CNDs showed excitation-dependent PL behavior upon irradiation with varying excitation wavelengths. The PL wavelength shifted from blue to red with increasing excitation wavelength. The emission maximum was observed at approximately 450 nm under excitation at 370 nm (Fig. 1b). This characteristic revealed that the PL of the CNDs depends on the surface state. The unique excitation-dependent PL behavior through the band-to-band transition of an electron in the conduction band to the valance band when a photon was emitted was induced by defects resulting from the entrapment of the generated excitons by surface passivation of the carbonized CNDs [33,34]. Through the integration sphere approach [35], the PLQY of the CND solution was 5.73%.

The photostability of the initially synthesized CNDs was determined by measuring PL intensities after 20 mW/cm$^2$ UV exposure in a dark room for 360 min. The PL intensity of the CNDs decreased by approximately 82% during the first 180 min, and was then maintained for the next 180 min (Fig. 2a). In Fig. 2b, the photostability of the CND solution that was stored in a refrigerator for 1.4 years is presented. Although the maximum PL value decreased by approximately 73% (normalized intensity = 0.73 at 0 min) compared with the initial value 1.4 years previously (normalized intensity = 1.0 at 0 min), the intensity under UV exposure was preserved at 92% for 37 h. The transmittance of CNDs dispersed in ultrapure water was measured to examine the blocking ratio in the UV-A wavelength range. As the wavelength range of the analytical instrument is limited to 360–740 nm, the transmittance of the CND solution could not be measured for the UV-B and UV-C regions. Therefore, a CNDs-PVA film was fabricated to demonstrate the UV-protective properties of the CNDs in the UV-B and UV-C regions (see section 3.3.). Fig. S2 shows the spectral light transmittance of the CND solution and ultrapure water without CNDs tested as a control. The mean transmittance of the CND solution from 360 nm to 400 nm was nearly 0%, whereas that of ultrapure water was approximately 100%. The UV-A blocking ratio of the CND solution was inferred from the transmittance values (Fig. 2c). The mean UV-A blocking ratio was 99.96% ± 0.08%. The CNDs fabricated in this study exhibit a higher blocking ratio than a commercial blue-blocking filter with a reported blocking ratio of 94.1% [36].

The morphology of the CNDs was explored by TEM imaging (Fig. 3a). The inlet of TEM images showed the lattice fringes with interplanar spacing of 0.39 nm, close to the (002) diffraction facets of graphite carbon, which is larger than that of graphite at 0.34 nm. This indicates the amorphous nature of the fabricated carbon dots. The quasi-spherical CNDs had sizes distributed between approximately 17 nm and 57 nm, with a peak around 32 nm, determined by counting 105 particles (Fig. 3b). CNDs are typically ~10 nm in size. Although the detailed chemical contents of *L. difformis* are still unclear, brown algae generally contain various polyphenolic compounds, including eckol, dieckol, and diphlorethohydroxycarmalol, polysaccharides like alginate, laminarin, fucoidan, and pigments such as β-carotene, chlorophyll, and fucoxanthin [37]. We suggest that the various organic materials in *L. difformis*, which were used as raw starting materials, operating temperature, and reaction time explain the amorphous nature of the CNDs with the larger and wider size range in this study. Several studies have shown that the degree of crystallinity, which is closely related to CND size, depends on the reaction time, synthesis temperature, starting materials as precursors, and initial concentrations of precursors [26,38]. In addition, the most recent research has demonstrated that some functional groups containing carboxyl groups affect particle size and quantum yield [39].

FT-IR was performed to determine the particle composition of freeze-dried CND powder. In Fig. 4, the O–H stretching peak is present at 3369.38 cm$^{-1}$ and another broad peak at 3000–3700 cm$^{-1}$, corresponding to the N–H stretching vibration, is observed overlapping the O–H peak. Owing to the broadening of the peaks of O–H and N–H, $sp^3$ C–H stretching of aliphatic compounds is shown marginally at 2941.68 cm$^{-1}$ [40]. The peaks at 1637.94 cm$^{-1}$ and 1414.09 cm$^{-1}$ correspond to C=O stretching and O–H bending, respectively. The strong and sharp absorption peaks at 1134.72 cm$^{-1}$ and 1107.81 cm$^{-1}$ represent C–N stretching and C–O stretching related to amine groups and secondary alcohol, respectively. The peak at 997.01 cm$^{-1}$ corresponds to C=C bending of aliphatic alkene. In addition, XPS was carried out to further verify the FT-IR assignments (Fig. 5). According to XPS, C (285.06 eV), O (532.85 eV), small amounts of N (400.28 eV), and some residual elements, including Cl, Mg, Na, Si, and S that were not completely washed out from the collected *L. difformis*, were identified (Fig. 5a). Their atomic ratios were C 45.64%, O 32.47%, N 4.39%, Cl 5.56%, Mg 3.66%, Na 3.22%, Si 2.72%, and S 2.35%. The high-resolution XPS spectra of C1s, O1s, and N1s are displayed in Fig. 5b–d. C1s has three peaks at 284.61 eV, 286.10 eV, and 288.0 eV corresponding to $sp^2$ C–C/C=C, $sp^3$ C-O/C-N, and carbonyl C=O, respectively. The high-resolution O1s spectrum has four peaks at 530.74 eV, 531.84 eV, 532.96 eV, and 535.67 eV, assigned to carbonate minerals as impurities, C=O, C-O, and auger peak of Na KLL, respectively. The de-convoluted N1s spectrum displays three peaks at 397.75 eV, 399.65 eV, and 401.02 eV, which are attributed to nitride compounds as impurities, amino N, and pyrrolic N, respectively. From the results, there are carbonyl, hydroxyl, and amino

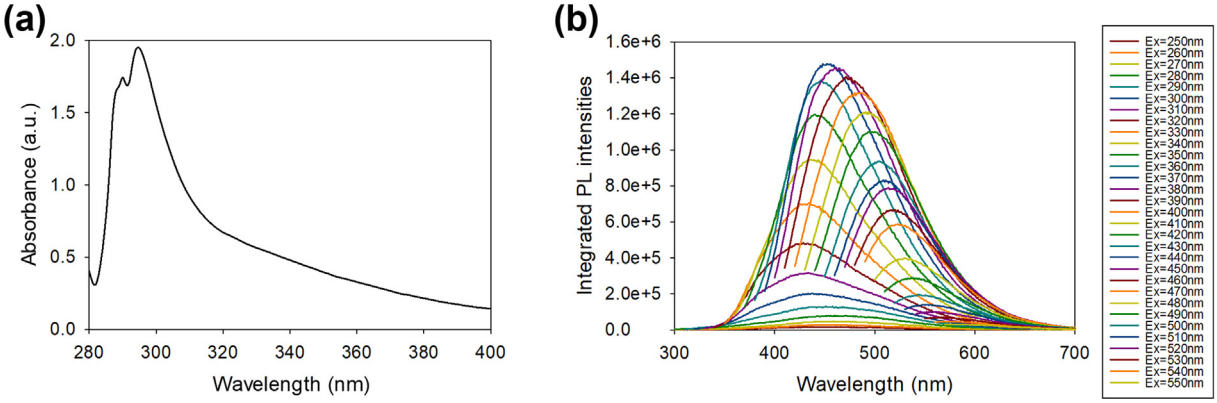


**Fig. 1.** (a) UV–vis absorption spectra of CNDs; (b) PL emission spectra under increasing excitation wavelength with 10-nm increments from 250 nm to 550 nm.

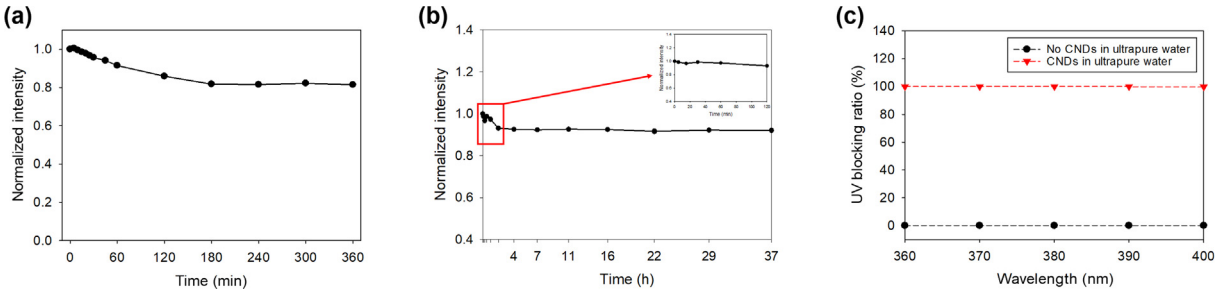


**Fig. 2.** (a) Evaluation of the photostability of CND solution under UV irradiation for 360 min; (b) Second evaluation of the photostability of CND solution under UV irradiation for 37 h after 1.4 years from an initial synthesis; (c) UV blocking ratio of CND solution within the UV-A range.

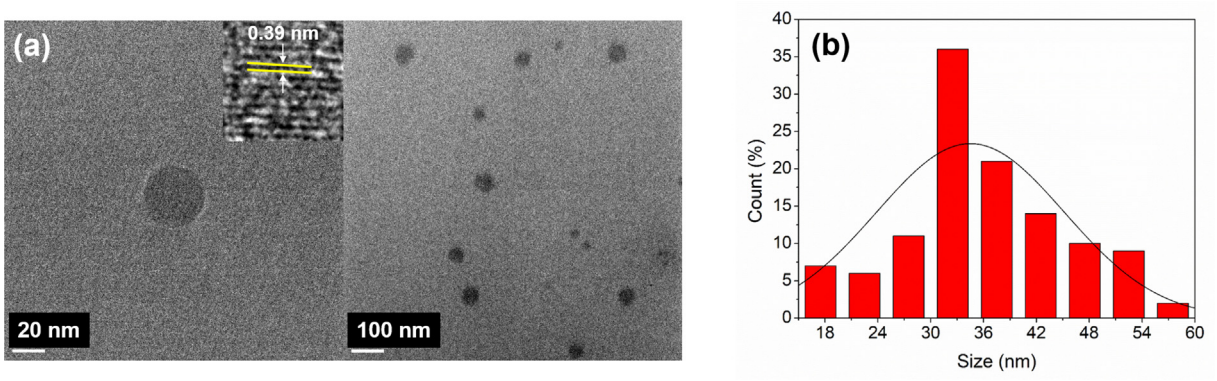


**Fig. 3.** (a) High-resolution TEM images of *L. diffformis*-based CNDs; (b) Size distribution of the as-synthesized CNDs.

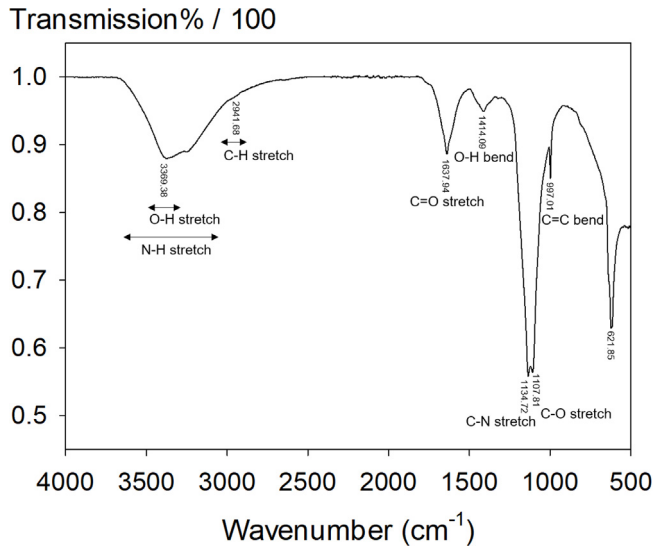


**Fig. 4.** FT-IR analysis of *L. diffformis*-based CNDs.

groups on the surface of the CNDs [41,42,43]. The functional groups of the CNDs fabricated from *L. diffformis* containing multiple carbon precursors serve as a passivation layer on the CND surface and contribute to the hydrophilicity and above-mentioned PL properties.

### 3.2. Optical characteristics of CNDs-PVA film

A PVA film including CNDs was prepared as mentioned above (see section 2.4.) to study its transmittance. The mean thickness of CNDs-PVA and PVA films was 0.136 mm and 0.130 mm, respectively. The CNDs-PVA film was sufficiently transparent to allow reading text underneath the film (Fig. 6a). Specific light-transmitting and wide-angle-light-scattering of planar sections of CNDs-PVA film and PVA film were tested according to ASTM D1003. The total transmittance of the CNDs-PVA and PVA films was 84.12% and 92.54%, respectively. Parallel light transmittance means that the ratio of the light passing through the films and the diffuse light transmittance is equal to the ratio of the light diffused through the films (Fig. 6b). Total light transmittance is the sum of the parallel light transmittance and the diffuse light transmittance. The transparency of the object is determined by the total light transmittance [44,45]. Incident light was diffused substantially more by and substantially less well penetrated CNDs-PVA film than PVA film (Table 1). Based on the results, we estimate that some of the incident light was influenced by the CNDs in the film. Because the CNDs can be excited by broadband light like the incident light, it is assumed that the effect was applied to the $T_p$ value. Although the total light transmittance, determining the transparency of the film, did not reach >90%, it differed by only 9% from that of the PVA film. The fluorescence emission of CNDs is highly excitation-dependent with good stability [33,46]. The CNDs-PVA film still maintained fluorescence emission under excitation with 430–440 nm of light even after it was kept without any thermo-hygrostat controller for 1.4 years (Fig. 6). Because the fluorescent CNDs in the film were durable, the CNDs-PVA film still showed UV-resistance performance. The UV blocking tests for UV-A and C regions were performed immediately after the films were fabricated, whereas the experiment upon UV-B region was performed using the film after 1.4 years.

### 3.3. Application of CNDs-PVA film for UV-C blocking

TRCDA vesicles are interesting materials characterized by color-shifting characteristics from blue to red upon external stimuli, such

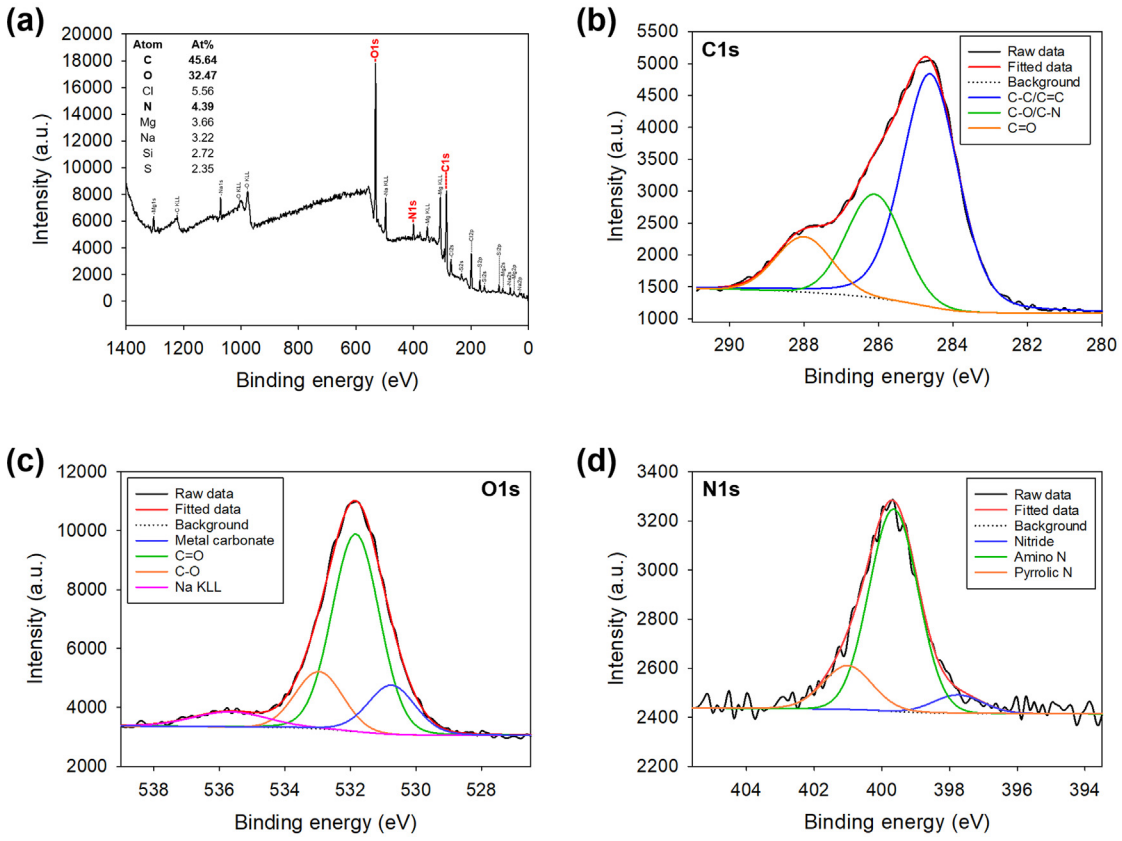


**Fig. 5.** (a) XPS survey spectrum of *L. differmis*-based CNDs; High-resolution XPS spectra of (b) C1s; (c) O1s; (d) N1s.

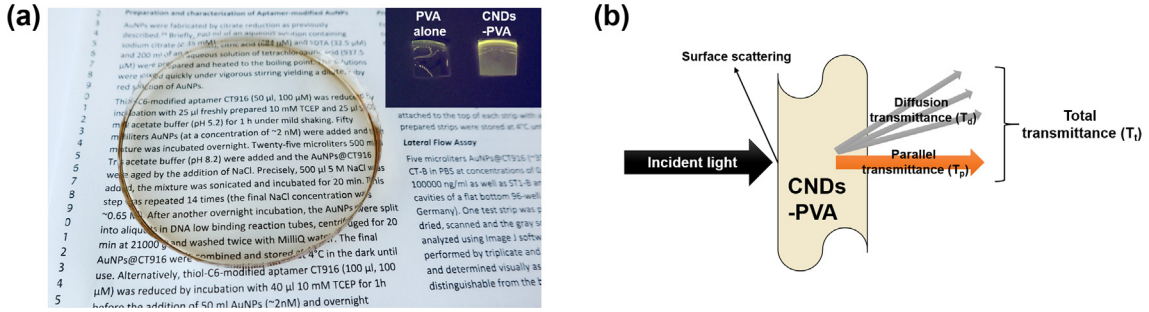


**Fig. 6.** (a) Image of a transparent CNDs-PVA composite film and its fluorescence emission under 430–440 nm after 1.4 years (inset); (b) Illustration of total transmittance ($T_t$) to qualify the transparency of CNDs.

**Table 1**
Transmittance of CNDs-PVA film and PVA film.

| Sample | Thickness (mm) | $T_t$ (%)[1] | $T_p$ (%)[2] | $T_d$ (%)[3] |
|---|---|---|---|---|
| CNDs-PVA | 0.136 | 84.12 ± 0.91 | 34.25 ± 2.62 | 49.87 ± 1.80 |
| PVA | 0.130 | 92.54 ± 0.08 | 89.72 ± 1.61 | 2.83 ± 1.53 |

[1]Total light transmittance, [2]parallel light transmittance, [3]diffuse light transmittance
*Total light transmittance = Parallel light transmittance + Diffuse light transmittance

as heat, light, pH, and biological/chemical recognition. To activate the characteristic color transition, the vesicles have to undergo polymerization by UV irradiation at 254 nm (UV-C) [32]. A TRCDA vesicle solution was prepared using ultrapure water. Freshly prepared vesicle solution was opaque whitish, whereas the solution turned blue after polymerization. Therefore, CR% (blue) values were calculated as an indirect index of protection ability against UV-C by the density of blue color when exposed to the UV-C light. In other words, if the CR% (blue) after UV irradiation is high, UV protection has not been achieved. On the contrary, if the CR% (blue) is low, UV protection has been accomplished (Fig. 7a). Two glass vials containing TRCDA vesicle solution were prepared; one vial was wrapped with CNDs-PVA film, and the other with PVA film. After exposure to UV-C light for 5 min, the two vials were

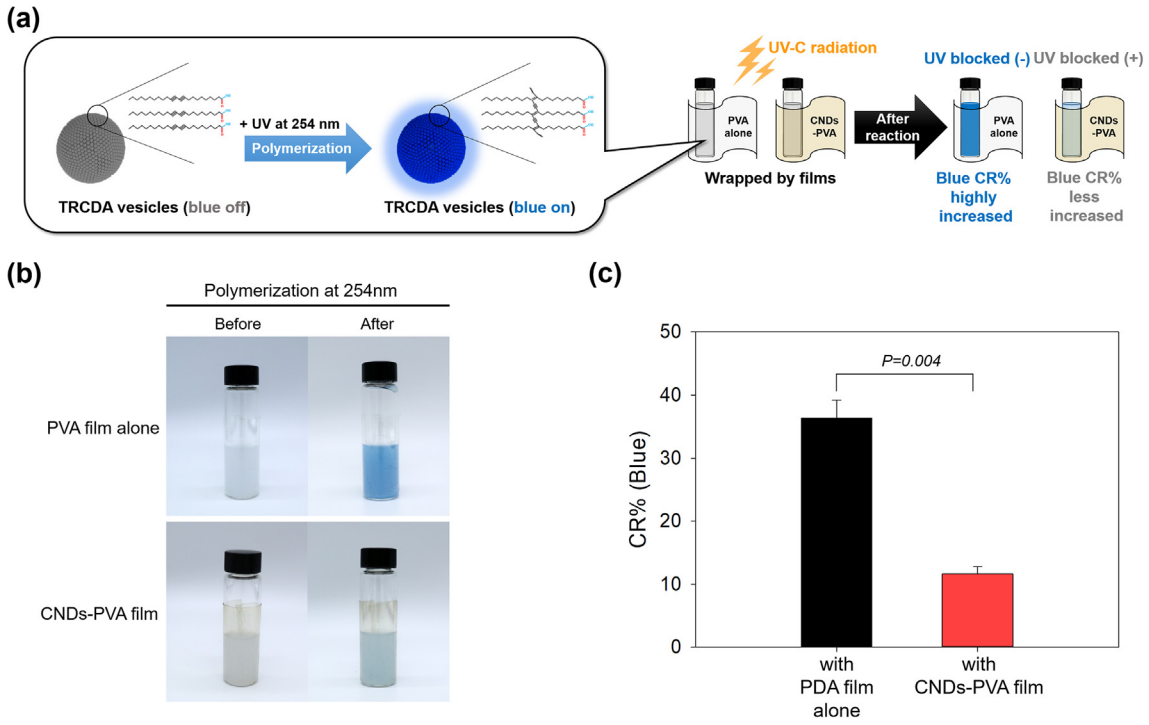


**Fig. 7.** (a) Schematic illustration of (a) UV-C blocking test based on color-transitional TRCDA vesicle solution; (b) Images of polymerization of TRCDA vesicle solution with or without CNDs-PVA film; (c) CR% of polymerized TRCDA vesicle solution.

compared. The vesicle solution in the vial wrapped with PVA film turned blue, whereas the solution in the vial wrapped with CNDs-PVA film showed a substantially limited color shift (Fig. 7b). To quantitatively represent the lower polymerization level of TRCDA in the vial wrapped with CNDs-PVA film, the CR% (blue) was calculated using Equation (1) [47]:

$$CR\% = \frac{PG_0 - PG_f}{PG_0} \times 100\% \quad (1)$$

where $PG_0$ is the initial gray level (%) of the solution before polymerization and $PG_f$ is the final gray level (%) after polymerization induced by UV exposure. The CR% (blue) of TRCDA vesicles in the

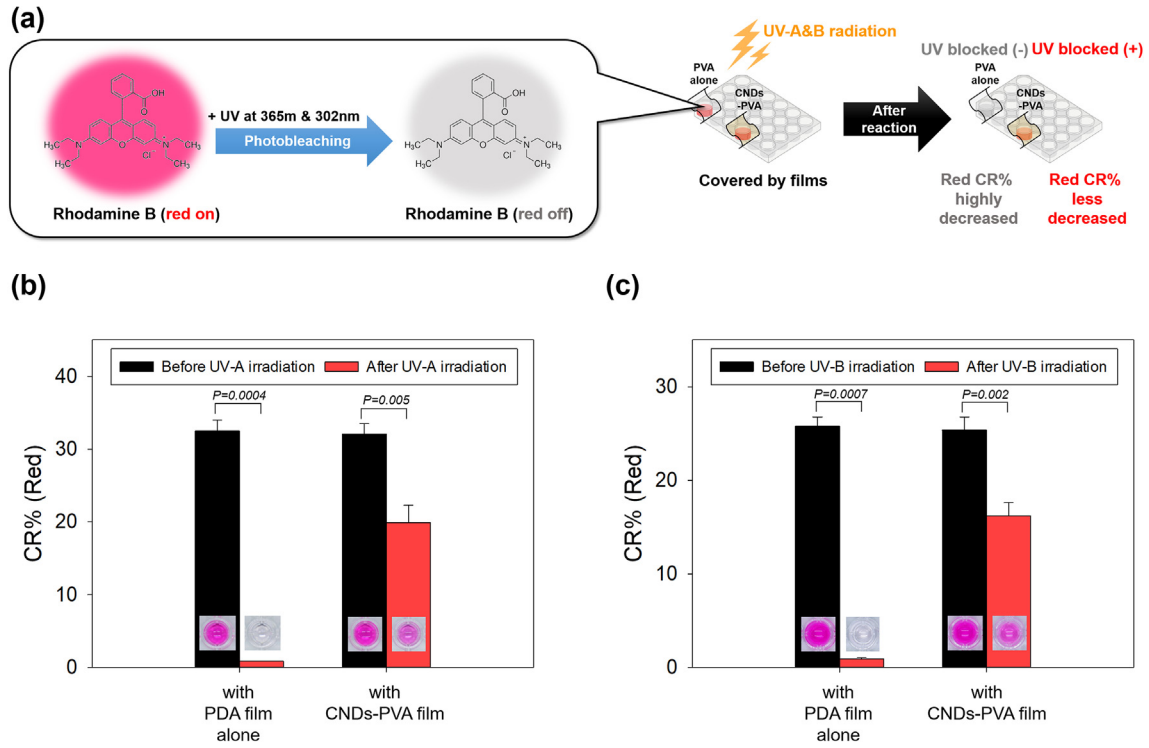


**Fig. 8.** (a) Schematic illustration of UV-A&B blocking test with Rhodamine B solution; (b) CR% of bleached rhodamine B solution with CNDs-PVA film under UV-A; (c) UV-B irradiation.

vial with PVA film was nearly four times higher than that of vesicles in the vial with CNDs-PVA film ($p$ = 0.004; Fig. 7c). In other words, the CNDs-PVA film blocked 30% more UV-C rays than the PVA film, confirming that the polymerization of TRCDA vesicles under UV-C light was effectively hindered by the CNDs-PVA film. Fig. S3 shows the specific color transition of TRCDA vesicles from blue to red upon external stimuli, ensuring that they were well-fabricated and validly used as a UV-C blocking indicator. The use of UV-C devices is historically limited to sterilization purposes, for example, in the food industry [48]. However, their use for germicidal purposes, i.e., to kill bacteria or viruses, has been substantially increasing recently owing to the increase in epidemics [49]. Based on the UV-C blocking results, we believe that the fabricated CNDs have strong potential as materials for UV-C light protection.

### 3.4. Application of CNDs-PVA film for UV-A and UV-B blocking

To evaluate the UV-A- and UV-B-protective features of CNDs-PVA film, we used a specific dye, red-colored rhodamine B that shows apparent photobleaching by UV irradiation. Prepared 1% of rhodamine B solution in wells covered with PVA film was extensively photo-bleached by UV-A as well as UV-B light, whereas that in wells covered with CNDs-PVA film was substantially less bleached (Fig. 8a). To quantitatively visualize the photobleaching of rhodamine B solution with or without CNDs-PVA film, CR% (red) values were calculated using the above formula (Fig. 8b-c) for the same purpose, with $PG_0$ being the initial gray level (%) of empty wells and $PG_f$ the final gray level (%) in the wells containing rhodamine B solution before and after UV exposure, respectively. In this case, if the CR% (red) after UV exposure is still high, UV protection has been achieved. CR% (red) values of rhodamine B solution with CNDs-PVA film and PVA film were 32.52% ± 1.48% and 32.08% ± 1.41%, respectively, before UV-A exposure at 365 nm. After UV-A irradiation for 3 h, the values decreased to 0.85% ± 0.05% and 19.88% ± 2.41%, respectively ($p$ = 0.0004 and $p$ = 0.005). In the case of PVA film, the value decreased by nearly 97%, whereas with CNDs-PVA film, it declined by only 38%. Upon UV-B exposure at 302 nm, the CR% (red) values of the rhodamine B solution decreased from 25.79% ± 0.98% to 0.92% ± 0.10% and from 25.36% ± 1.41% to 16.20% ± 1.42%, respectively, indicating 96% and 36% decreases from the initial value ($p$ = 0.0007 and $p$ = 0.002). These results suggest that CNDs-PVA film also effectively blocks at least >60% of UV-A and UV-B rays.

This study had some limitations. First, this was a prospective laboratory study, with preliminary results. Although CNDs from natural resources are generally eco-friendly and have low cytotoxicity, further studies, including cytotoxicity tests, are required before the application of CNDs from *L. difformis* in commercial UV films and sunblock agents can be considered.

## 4. Conclusions

We successfully synthesized CNDs and a CNDs-PVA film that protect against UV-A, UV-B, and UV-C rays from sea cauliflower, *L. difformis*, which has little utility value. The synthesis of CNDs is simple, environmentally friendly, and cost-effective, and CNDs readily form in aqueous solution by heat treatment. In the initial synthesis, the CNDs exhibited sufficient photostability even under direct and strong UV-A ray exposure, and still showed good photostability after 1.4 years. The CNDs-PVA film also demonstrated good UV-protective performance upon UV light irradiation. Furthermore, the UV-blocking CNDs-PVA film exhibited good transparency and flexibility, maintained the inherent characteristics of CNDs, and was easily prepared by the direct mixing of CND and PVA solutions, without a need for further treatment or purification. As the industrial and commercial use of UV-protective agents will likely continue to increase, these marine-based CNDs and derived composite films have wide application potential. To this date, it remains unknown how many species live in the vast oceans of the Earth. Accordingly, marine organisms and marine biotechnology are still extremely underexplored. This work was a first attempt and a proof-of-concept study to use an under- or unutilized marine brown alga found in South Korea in the development of a UV-blocking natural material. In future studies, CNDs can be synthesized, functionalized, and customized from countless hitherto veiled marine organisms, increasing the enormous potential of marine biotechnology in many research and industrial fields.

## Financial support

This work was supported by the National Marine Biodiversity Institute of Korea (MABIK) [grant number: 2021M00600].

## Patents

A Korean patent application has been filed for the contents described in this paper (patent number 10-2020-0051362).

## Conflict of interest

The authors declare that they have no conflict of interest.

## Supplementary material

https://doi.org/10.1016/j.ejbt.2021.12.004.

## References

[1] Bosch R, Phillips N, Suárez-Pérez JA, et al. Mechanisms of photoaging and cutaneous photocarcinogenesis, and photoprotective strategies with phytochemicals. Antioxidants 2015;4:246–68. https://doi.org/10.3390/antiox4020248 PMid: 26783703.
[2] D'Orazio J, Jarrett S, Amaro-Ortiz A, et al. UV radiation and the skin. Int J Mol Sci 2013;14:12222–48. https://doi.org/10.3390/ijms140612222 PMid: 23749111.
[3] Li Y, Hou X, Yang C, et al. Photoprotection of cerium oxide nanoparticles against UVA radiation-induced senescence of human skin fibroblasts due to their antioxidant properties. Sci Rep 2019;9:2595. https://doi.org/10.1038/s41598-019-39486-7 PMid:30796322.
[4] Deng Y, Ediriwickrema A, Yang F, et al. A sunblock based on bioadhesive nanoparticles. Nat Mater 2015;14:1278–85. https://doi.org/10.1038/nmat4422 PMid: 26413985.
[5] Pillai S, Oresajo C, Hayward J. Ultraviolet radiation and skin aging: roles of reactive oxygen species, inflammation and protease activation, and strategies for prevention of inflammation-induced matrix degradation - a review. Int J Cosmet Sci 2005;27:17–34. https://doi.org/10.1111/j.1467-2494.2004.00241.x PMid: 18492178.
[6] Mates JM, Perez-Gomez C, Nunez de Castro I. Antioxidant enzymes and human diseases. Clin Biochem 1999;32:595–603. https://doi.org/10.1016/S0009-9120(99)00075-2.
[7] Narayanan DL, Saladi RN, Fox JL. Ultraviolet radiation and skin cancer. Int J Dermatol 2010;49:978–86. https://doi.org/10.1111/j.1365-4632.2010.04474.x PMid:20883261.
[8] Smijs TG, Pavel S. Titanium dioxide and zinc oxide nanoparticles in sunscreens: focus on their safety and effectiveness. Nanotechnol Sci Appl 2011;4:95–112. https://doi.org/10.2147/NSA.S19419 PMid: 24198489.
[9] Suh HW, Lewis J, Fong L, et al. Biodegradable bioadhesive nanoparticle incorporation of broad-spectrum organic sunscreen agents. Bioeng Transl Med 2019;4:129–40. https://doi.org/10.1002/btm2.10092 PMid: 30680324.
[10] Hanson KM, Gratton E, Bardeen CJ. Sunscreen enhancement of UV-induced reactive oxygen species in the skin. Free Radic Biol Med 2006;41:1205–12. https://doi.org/10.1016/j.freeradbiomed.2006.06.011 PMid: 17015167.
[11] Rass K, Reichrath J. UV damage and DNA repair in malignant melanoma and nonmelanoma skin cancer. Adv Exp Med Biol 2008;624:162–78. https://doi.org/10.1007/978-0-387-77574-6_13 PMid: 18348455.
[12] Spratt EAG, Carucci JA. Skin cancer in immunosuppressed patients. Facial Plast Surg 2013;29:402–10. https://doi.org/10.1055/s-0033-1353381 PMid: 24037934.
[13] Piccinino D, Capecchi E, Tomaino E, et al. Nano-structured lignin as green antioxidant and UV shielding ingredient for sunscreen applications.

Antioxidants (Basel) 2021;10:274. https://doi.org/10.3390/antiox10020274 PMid: 33578879.
[14] Tovar-Sanchez A, Sanchez-Quiles D, Basterretxea G, et al. Sunscreen products as emerging pollutants to coastal waters. PLoS One 2013;8:e65451. https://doi.org/10.1371/journal.pone.0065451 PMid: 23755233.
[15] Widsten P, Tamminen T, Liitia T. Natural sunscreens based on nanoparticles of modified kraft lignin (CatLignin). ACS Omega 2020;5:13438–46. https://doi.org/10.1021/acsomega.0c01742 PMid: 32548532.
[16] Ouchene L, Litvinov IV, Netchiporouk E. Hawaii and other jurisdictions ban oxybenzone or octinoxate sunscreens based on the confirmed adverse environmental effects of sunscreen ingredients on aquatic environments. J Cutan Med Surg 2019;23:648–9. https://doi.org/10.1177/1203475419871592 PMid: 31729915.
[17] Chatzimitakos TG, Kasouni A, Troganis A, et al. Carbon nanodots synthesized from *Dunaliella salina* as sun protection filters. C J Carbon Res 2020;6:69. https://doi.org/10.3390/c6040069.
[18] Carbonaro CM, Corpino R, Salis M, et al. On the emission properties of carbon dots: reviewing data and discussing models. C J Carbon Res 2019;5:60. https://doi.org/10.3390/c5040060.
[19] Hess SC, Permatasari FA, Fukazawa H, et al. Direct synthesis of carbon quantum dots in aqueous polymer solution: one-pot reaction and preparation of transparent UV-blocking films. J Mater Chem A 2017;5:5187–94. https://doi.org/10.1039/C7TA00397H.
[20] Hu G, Lei B, Jiao X, et al. Synthesis of modified carbon dots with performance of ultraviolet absorption used in sunscreen. Opt Express 2019;27:7629–41. https://doi.org/10.1364/OE.27.007629 PMid: 30876325.
[21] Kasouni A, Chatzimitakos T, Stalikas C. Bioimaging applications of carbon nanodots: a review. C J Carbon Res 2019;5:19. https://doi.org/10.3390/c5020019.
[22] Li H, Kang Z, Liu Y, et al. Carbon nanodots: synthesis, properties and applications. J Mater Chem 2012;22:24230–53. https://doi.org/10.1039/c2jm34690g.
[23] Chan KK, Yap SHK, Yong KT. Biogreen synthesis of carbon dots for biotechnology and nanomedicine applications. Nanomicro Lett 2018;10:72. https://doi.org/10.1007/s40820-018-0223-3 PMid: 30417004.
[24] Das R, Bandyopadhyay R, Pramanik P. Carbon quantum dots from natural resource: a review. Mater Today Chem 2018;8:96–109. https://doi.org/10.1016/j.mtchem.2018.03.003.
[25] Wang R, Lu K-Q, Tang Z-R, et al. Recent progress in carbon quantum dots: synthesis, properties and applications in photocatalysis. J Mater Chem A 2017;5:3717–34. https://doi.org/10.1039/C6TA08660H.
[26] Kim KW, Choi T-Y, Kwon YM, et al. Simple synthesis of photoluminescent carbon dots from a marine polysaccharide found in shark cartilage. Electron J Biotechnol 2020;47:36–42. https://doi.org/10.1016/j.ejbt.2020.07.003.
[27] Pawar S, Togiti UK, Bhattacharya A, et al. Functionalized chitosan-carbon dots: a fluorescent probe for detecting trace amount of water in organic solvents. ACS Omega 2019;4:11301–11. https://doi.org/10.1021/acsomega.9b01208 PMid: 31460233.
[28] Godavarthi S, Mohan Kumar K, Vázquez Vélez E, et al. Nitrogen doped carbon dots derived from *Sargassum fluitans* as fluorophore for DNA detection. J Photochem Photobiol B 2017;172:36–41. https://doi.org/10.1016/j.jphotobiol.2017.05.014 PMid: 28514712.
[29] Feng X, Zhao Y, Jiang Y, et al. Use of carbon dots to enhance UV-blocking of transparent nanocellulose films. Carbohydr Polym 2017;161:253–60. https://doi.org/10.1016/j.carbpol.2017.01.030 PMid: 28189236.
[30] Zuo D, Liang N, Xu J, et al. UV protection from cotton fabrics finished with boron and nitrogen co-doped carbon dots. Cellulose 2019;26:4205–12. https://doi.org/10.1007/s10570-019-02365-5.
[31] Kwon S, Orsuwan A, Bumbudsanpharoke N, et al. A Short review of light barrier materials for food and beverage packaging. Korean J Packag Sci Tech 2018;24:141–8. https://doi.org/10.20909/kopast.2018.24.3.141.
[32] Okada S, Peng S, Spevak W, et al. Color and chromism of polydiacetylene vesicles. Acc Chem Res 1998;31:229–39. https://doi.org/10.1021/ar970063v.
[33] Sahu S, Behera B, Maiti TK, et al. Simple one-step synthesis of highly luminescent carbon dots from orange juice: application as excellent bio-imaging agents. Chem Commun (Camb) 2012;48:8835–7. https://doi.org/10.1039/c2cc33796g PMid: 22836910.
[34] Yang Y, Cui J, Zheng M, et al. One-step synthesis of amino-functionalized fluorescent carbon nanoparticles by hydrothermal carbonization of chitosan. Chem Commun (Camb) 2012;48:380–2. https://doi.org/10.1039/C1CC15678K PMid: 22080285.
[35] de Mello JC, Wittmann HF, Friend RH. An improved experimental determination of external photoluminescence quantum efficiency. Adv Mater 1997;9:230–2. https://doi.org/10.1002/adma.19970090308.
[36] Park SJ, Yang HK, Moon BK. Ultraviolet to blue blocking and wavelength convertible films using carbon dots for interrupting eye damage caused by general lighting. Nano Energy 2019;60:87–94. https://doi.org/10.1016/j.nanoen.2019.03.043.
[37] Kim T-H, Jung W-K. R&D trends of brown algae as potential candidates in biomedical application. J Mar Biosci Biotechnol 2019;11:1–13. https://doi.org/10.15433/ksmb.2019.11.1.001.
[38] Papaioannou N, Titirici MM, Sapelkin A. Investigating the effect of reaction time on carbon dot formation, structure, and optical properties. ACS Omega 2019;4:21658–65. https://doi.org/10.1021/acsomega.9b01798 PMid: 31891043.
[39] Javed N, O'Carroll DM. Long-term effects of impurities on the particles size and optical emission of carbon dots. Nanoscale Adv 2021;3:182–9. https://doi.org/10.1039/D0NA00479K.
[40] Tomskaya AE, Egorova MN, Kapitonov AN, et al. Synthesis of luminescent N-doped carbon dots by hydrothermal treatment. Physica Status Solidi B 2018;255:1700222. https://doi.org/10.1002/pssb.201700222.
[41] Kuo W-S, Chang C-Y, Huang K-S, et al. Amino-functionalized nitrogen-doped graphene-quantum-dot-based nanomaterials with nitrogen and amino-functionalized group content dependence for highly efficient two-photon bioimaging. Int J Mol Sci 2020;21:2939. https://doi.org/10.3390/ijms21082939 PMid: 32331302.
[42] Liu Q, Zhang N, Shi H, et al. One-step microwave synthesis of carbon dots for highly sensitive and selective detection of copper ion in aqueous solution. New J Chem 2018;42:3097–101. https://doi.org/10.1039/C7NJ05000C.
[43] Liu W, Li C, Sun X, et al. Highly crystalline carbon dots from fresh tomato: UV emission and quantum confinement. Nanotechnology 2017;28. https://doi.org/10.1088/1361-6528/aa900b PMid: 28961145.
[44] Webber AC. Method for the measurement of transparency of sheet materials. J Opt Soc Am 1957;47:785–9. https://doi.org/10.1364/JOSA.47.000785.
[45] Kato A, Ikeda Y, Kasahara Y, et al. Optical transparency and silica network structure in cross-linked natural rubber as revealed by spectroscopic and three-dimensional transmission electron microscopy techniques. J Opt Soc Am B 2008;25:1602–15. https://doi.org/10.1364/JOSAB.25.001602.
[46] Asmaa ME-S. Carbon dots: Discovery, structure, fluorescent properties, and applications. Green Process Synth 2021;10:134–56. https://doi.org/10.1515/gps-2021-0006.
[47] Kim KW, Lee JM, Kwon YM, et al. Polyamine-functionalized polydiacetylene (PDA) vesicles for colorimetric sensing of carbon dioxide. Macromol Res 2018;26:284–90. https://doi.org/10.1007/s13233-018-6036-x.
[48] Singh H, Bhardwaj SK, Khatri M, et al. UVC radiation for food safety: an emerging technology for the microbial disinfection of food products. Chem Eng Sci 2021;417:128084. https://doi.org/10.1016/j.cej.2020.128084.
[49] Schnell E, Karamooz E, Harriff MJ, et al. Construction and validation of an ultraviolet germicidal irradiation system using locally available components. PLoS ONE 2021;16:e0255123. https://doi.org/10.1371/journal.pone.0255123 PMid: 34297764.